

Fracture behavior of Al-0.2wt%Zr alloy processed by accumulative roll-bonding (ARB) process

B. Azad¹, E. Borhani^{2*}, H. M. Semnani¹

¹Faculty of Metallurgical and Materials Engineering, Semnan University, Semnan, Iran

²Department of Nanotechnology, Nano-Materials Group, Semnan University, Semnan, Iran

Received 3 July 2014, received in revised form 12 December 2014, accepted 26 February 2015

Abstract

An Al-0.2wt%Zr alloy was subjected to accumulative roll-bonding (ARB) process up to a strain of 8.0. The aim of this study is to investigate the fracture surfaces of Al-0.2wt%Zr alloy fabricated by the ARB process. The three kinds of different microstructures, i.e. solution-treated, 350 °C pre-aged and 450 °C pre-aged ones, were prepared as the starting structures for the ARB process. Investigation of the fracture surfaces was carried out by scanning electron microscope (SEM). Also, the microstructure evolution after the ARB process were studied by atomic force microscope (AFM).

Key words: Al-0.2wt%Zr alloy, accumulative roll-bonding (ARB) process, fracture surfaces

1. Introduction

The severe plastic deformation (SPD) processes were developed to achieve ultrafine grained (UFG) microstructure having a mean grain size smaller than 1 μm [1, 2]. Several methods were developed for SPD processes, which include equal channel angular pressing (ECAP) [3], accumulative roll bonding (ARB) [4], high-pressure torsion (HPT) [5], cyclic extrusion compression (CEC) [6], repetitive corrugation and straightening (RCS) [7]. The ARB process developed by Saito et al. [8] in 1998 is the only SPD process that can be applied to the continuous production of bulky sheet materials [9]. The ARB allows us to accumulate very large strains in materials without changing the initial dimensions of the materials by repeating the process of cutting the rolled sheets, stacking them to the initial thickness and roll bonding the stacked sheets again. The principle of the ARB is schematically shown in Fig. 1 [8]. The microstructure evolution, mechanical properties and texture evolution of ARB-processed alloys have been studied by many researchers [1, 9–15]. However, some characteristics of ARB-processed alloys such as fracture surfaces study still need in-depth research. The fracture study is

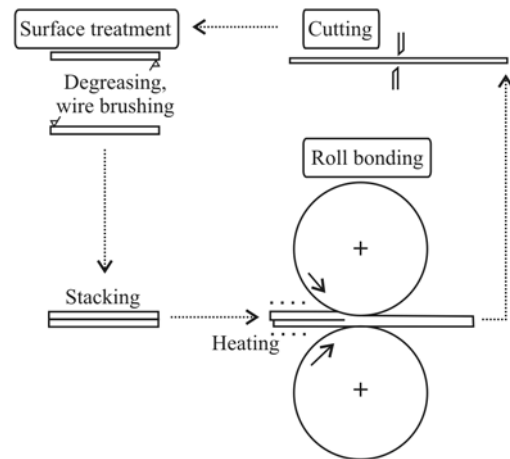


Fig. 1. Schematic illustration showing the principle of the ARB process [8].

important to clarify the rupture mechanisms in the ARB processed specimens.

In the present study, the ARB process was carried out on Al-0.2wt%Zr alloy having different starting microstructures to research on the fracture behavior

*Corresponding author: tel./fax: +982333654119; e-mail address: Ehsan.Borhani@profs.semnan.ac.ir

Table 1. Chemical composition of Al-0.2wt%Zr alloy (wt.%)

Elements	Zr	Fe	Si	Mg	Cu	Mn	Al
	0.208	0.004	0.002	0.001	0.002	0.001	Balance

of the alloy during the ARB process.

The Al-Zr system exhibits particular promise for developing thermally stable precipitation-strengthened aluminum alloys [16]. On the other hand, the properties of Al alloys often improve by Zr addition [17, 18]. In Al-Zr system, fine Al_3Zr particles precipitate within the matrix during aging from supersaturated solid solution. The precipitates are stable even at high temperatures and inhibit recrystallization and grain growth by pinning grain boundaries [16–18].

2. Materials and methods

The chemical composition of Al-0.2wt%Zr is given in Table 1. A binary Al-0.2wt%Zr alloy was prepared as sheets with a thickness of 2 mm, a width of 60 mm a length of 200 mm. The sheets were solution treated (ST) at 635 °C for 24 h and then immediately water-quenched. The average grain size of the matrix in the ST-sheets was 1.5 μm . Some of the ST-sheets were aged at 350 or 450 °C for 3 h, to have Al_3Zr precipitates. Sato et al. previously showed that Al_3Zr precipitates could be produced after aging process [19], therefore, after the aging process in this research probably Al_3Zr precipitates are formed in Al-0.2wt%Zr alloy with different size of precipitates due to different aging temperatures.

Figure 2 shows the schematic illustration of the thermal and mechanical processes used in this study.

Fractography was studied by scanning electron

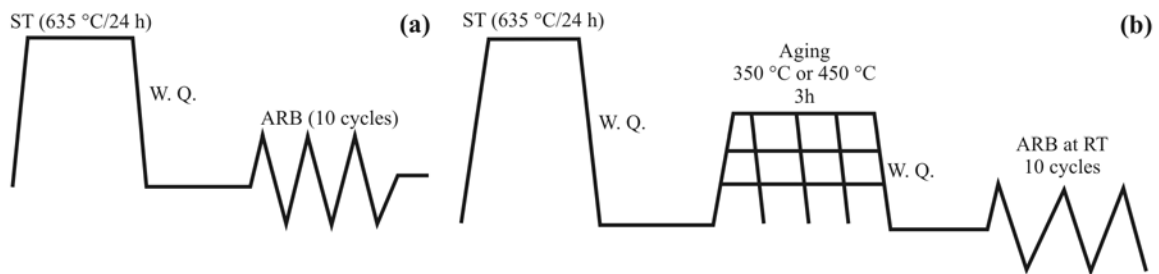


Fig. 2. Schematic illustration of the thermal and mechanical process used in this study.

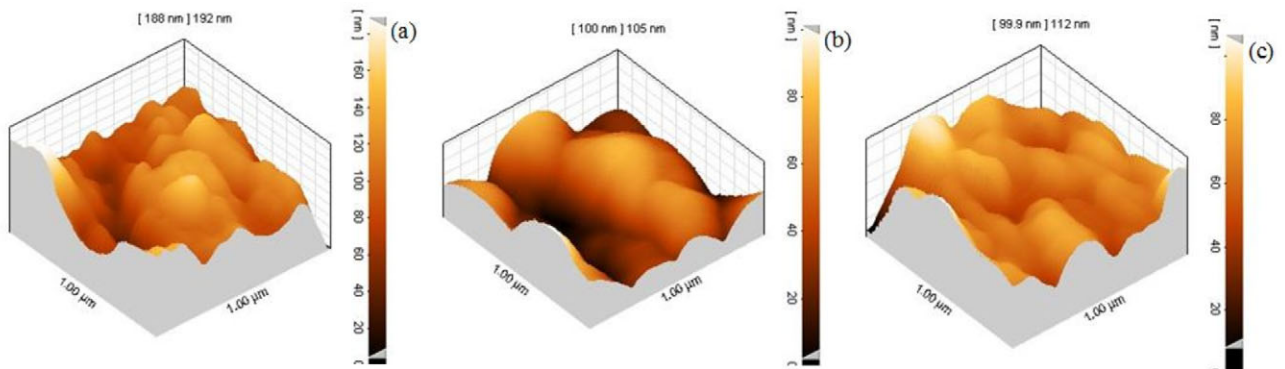


Fig. 3. AFM micrographs of TD planes after 1-cycle ARB: a) ST, b) 350 °C-Aged ARB, and c) 450 °C-Aged ARB specimens.

Table 2. The mean grain size after ARB process

The number of ARB cycles, N	The mean grain size (μm)		
	ST-ARB	350 °C Aged-ARB	450 °C Aged-ARB
1	1.5	0.9	1.2
10	0.4	0.3	0.32

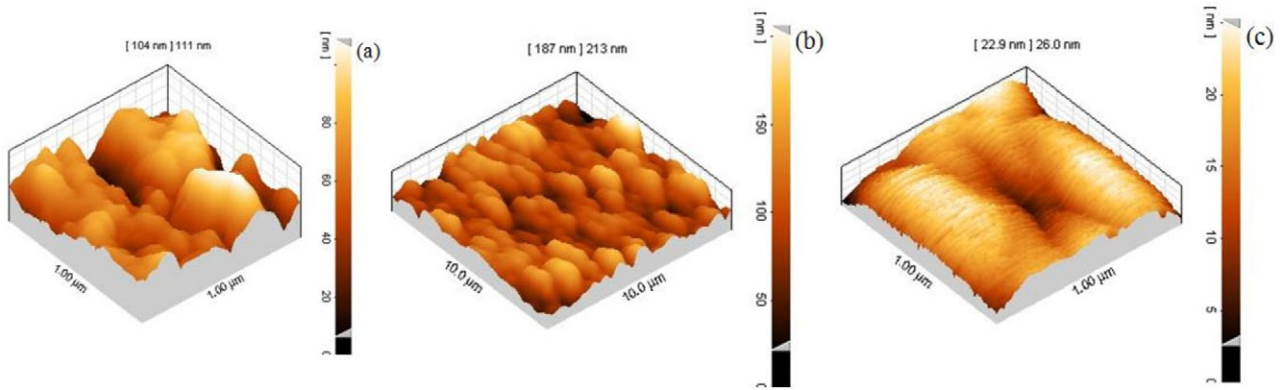


Fig. 4. AFM micrographs of TD planes after 10-cycle ARB: a) ST, b) 350°C-Aged ARB, and c) 450°C-Aged ARB specimens.

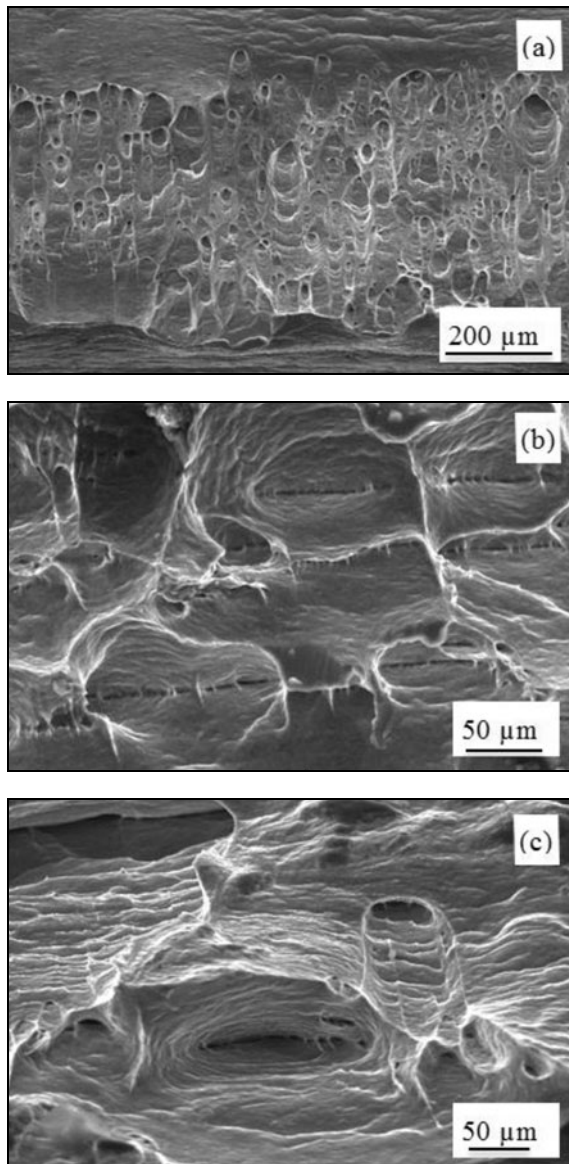


Fig. 5. Fracture surfaces after tensile test in a) ST, b) 350°C-Aged and c) 450°C-Aged specimens before the ARB process.

microscope (SEM). Also, the grain size of specimens during the ARB process for ST and Aged specimens was measured by atomic force microscope (AFM).

3. Results and discussion

AFM micrographs of the ST-ARB and Aged-ARB specimens from TD planes after 1 and 10 cycles of ARB process are shown in Figs. 3, 4.

The value of the mean grain size is also shown in Table 2. Figures 3, 4 and Table 2 clearly indicate that the mean grain size decreases with increasing the number of the ARB cycles in all the specimens. After 1-cycle ARB, the mean grain size of the ST-ARB, 350°C Aged-ARB and 450°C Aged-ARB specimens reaches 1.5, 0.9 and 1.2 μm , respectively. After 10-cycle ARB, the mean grain size of the ST-ARB, 350°C Aged-ARB and 450°C Aged-ARB specimens reaches 0.4, 0.3 and 0.32 μm , respectively.

Types of fractures can be roughly divided into two categories, which are brittle and ductile fractures [20]. Ductile and brittle fractures describe the amount of macroscopic plastic deformation that precedes fracture [21]. A ductile fracture occurs by microvoid formation and coalescence. The former has, however, gained much interest due to its catastrophic results whenever happens. A limited amount of plastic deformation occurring during brittle fracture promotes a sudden failure without warning. Ductile fracture, on the contrary, exhibits rough and dull fracture surfaces with gross plastic deformation, therefore allowing more time to correct or prevent such failure. Also, types of fractures can be described by transgranular fracture and intergranular fracture [20]. The transgranular fracture can be classified into brittle cleavage fracture, ductile fracture and fatigue fracture. Also, the intergranular fracture can be classified into intergranular fracture without microvoid and intergranular fracture with microvoid. A brittle fracture occurs by either transgranular or

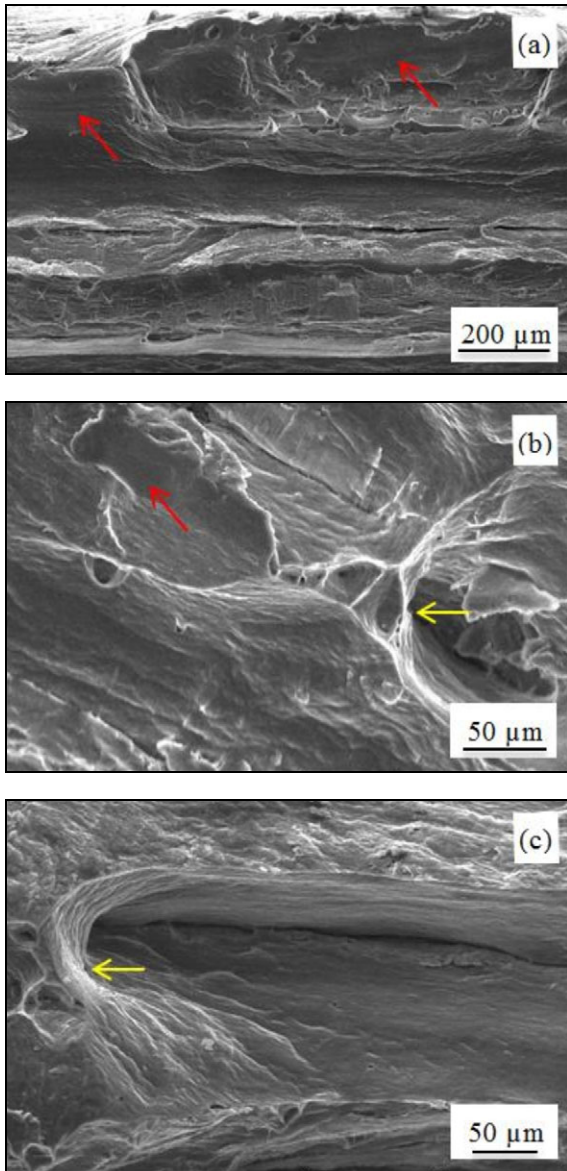


Fig. 6. Fracture surfaces after tensile test in a) ST, b) 350°C-Aged ARB, and c) 450°C-Aged ARB specimens after 3-cycle ARB process.

intergranular cracking [21]. Fracture surfaces of ST, 350°C Aged and 450°C Aged specimens before the ARB process are shown in Fig. 5, respectively.

Figure 5a shows the dimples indicating the microvoid coalescence (MVC) mechanism of ductile fracture before the ARB process. Whereas, Figs. 5b,c show transgranular cleavage fractures. The shape of the dimples can determine the type of loading the component has experienced during fracture, and the orientation of the dimples reveals the direction of crack extension [22]. Ductile fracture almost has a gray, fibrous appearance and equiaxed or hemispheroidal dimples [20, 23] which are clearly seen in Fig. 5a. Transgranular cleavage fracture is usually associated

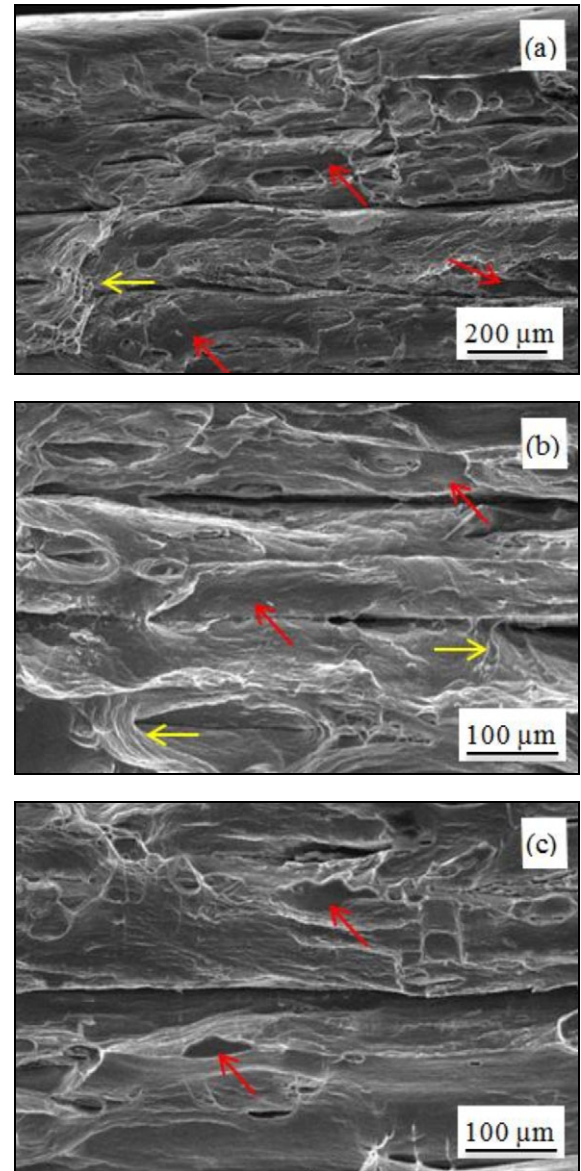


Fig. 7. Fracture surfaces after tensile test in a) ST, b) 350°C-Aged ARB, and c) 450°C-Aged ARB specimens after 7-cycle ARB process.

with defects such as cracks, porosity, inclusions or second phase particles in which dislocations movement is obstructed. This suggests precipitation of Al_3Zr at 350°C and 450°C in the specimen after aging process [19]. The obtained results are in good agreement with previous reports [21, 22].

The fracture surfaces of specimens after 3, 7 and 10 cycles of the ARB process are shown in Figs. 6, 7 and 8, respectively. After 3-cycle ARB (Fig. 6), the size of dimples are smaller compared to initial cycle and cleavage facets are clearly seen as indicated by red arrows. Ductile fractures can be detected in an annealed sample [20] that has been already reported [22]. Also, at Aged-ARB specimens

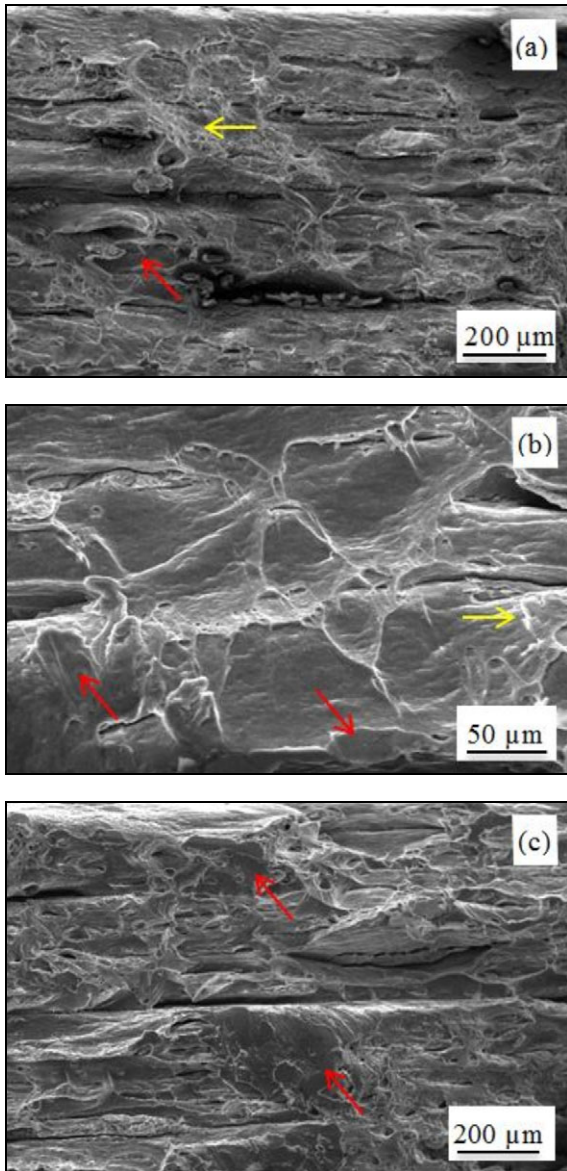


Fig. 8. Fracture surfaces after tensile test in a) ST, b) 350°C-Aged ARB, and c) 450°C-Aged ARB specimens after 10-cycle ARB process.

the cleavage facets and the river lines are seen. The river lines or the stress lines are steps between cleavage or parallel planes, which are always converged in the direction of local crack propagation. The river lines and the cleavage facets are indicated by yellow and red arrows, respectively. This direction is normally observed pointing to inclusion, porosity, crack or second-phase particle, which create stress concentration. Stress is therefore concentrated in front of these defects, initiating a crack of a critical size [20]. The propagation of this crack then finally causes the global failure with very little plastic deformation.

With increasing the number of ARB cycles, the brittle fracture can be detected. This result has been

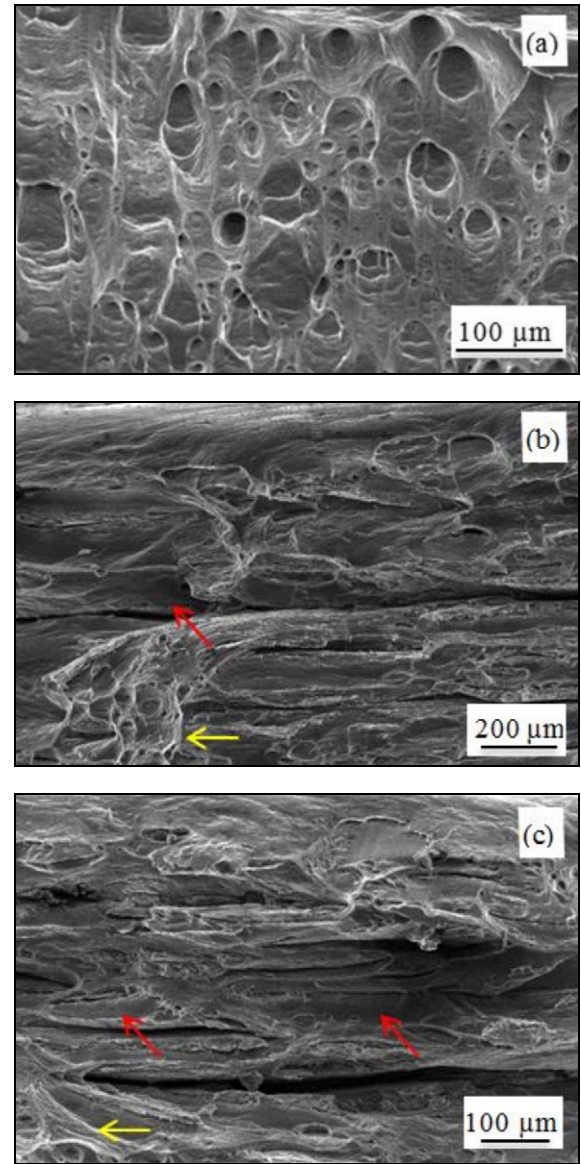


Fig. 9. Fracture surfaces in ST specimen after tensile test a) before ARB process, b) after 7-cycle, and c) after 10-cycle ARB process.

previously reported [21]. At ST-ARB specimen, with increasing the number of ARB cycles, the dimples are not as deep as in the initial material. After 7 and 10 cycles of ARB (Figs. 7, 8), at ST-ARB and Aged-ARB specimens, a brittle fracture is dominant. The river lines and the cleavage facets are seen at the specimens after 7 and 10 cycles of ARB. At the final cycle, the brittle fracture can be detected. The river lines and the cleavage facets are indicated by yellow and red arrows, respectively. It can be seen in Fig. 8a that the dimple size significantly decreases with increasing the number of ARB cycles.

In Figures 9a–c the fracture surfaces at a higher magnification are shown. The deep equiaxed dimples

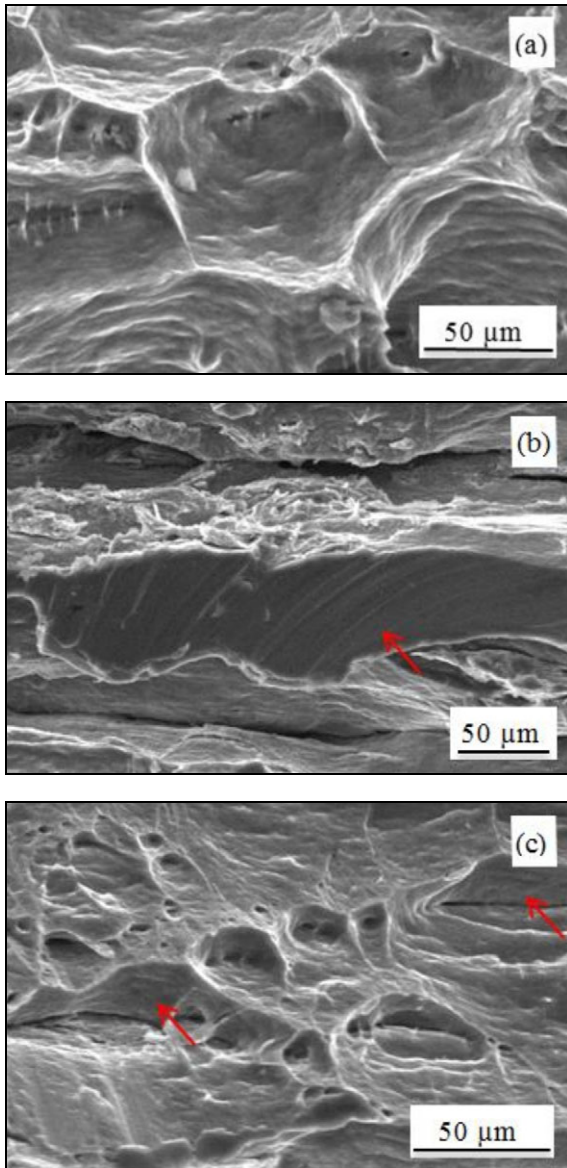


Fig. 10. Fracture surfaces in 350°C Aged-specimen after tensile test a) before ARB process, b) after 7-cycle, and c) after 10-cycle ARB process.

are clearly seen in the initial cycle (Fig. 9a), that cause a ductile fracture that occurs by nucleation of microvoids [20, 23]. Also, the river lines and the cleavage facets at the final cycles (Figs. 9b,c) are seen in ST specimens.

Also, the fracture surfaces of Aged-specimens are shown in Figs. 10 and 11. As can be seen in these figures, in the initial cycle the transgranular fracture is dominant because of the presence of the precipitates after the aging process. It is thought that there are interesting differences in aging and precipitation behavior between conventionally coarse-grained materials and UFG materials [9, 19]. With increasing the number of ARB cycles, it can be

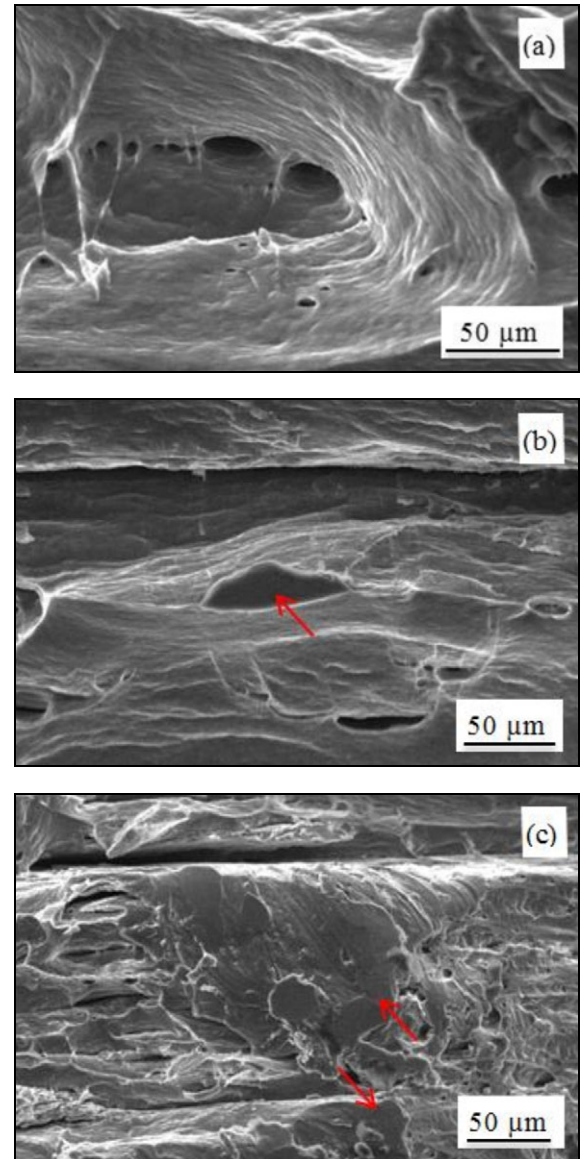


Fig. 11. Fracture surface in 450°C Aged-specimen after tensile test a) before ARB process, b) after 7-cycle, and c) after 10-cycle ARB process.

detected that a brittle fracture is dominant, and the cleavage facets are seen at the final cycles.

4. Conclusions

1. The mean grain size after 10-cycle of ARB in the ST-ARB, 350°C Aged-ARB, and 450°C Aged-ARB reached 0.4, 0.3 and 0.32 μm , respectively.

2. Fractography of Al-0.2wt%Zr alloy showed that at initial cycles the ductile fracture and at final cycles the brittle fracture were detected.

3. Before the ARB process, in the ST and the Aged specimens, the ductile fracture and transgran-

ular cleavage facets were detected, respectively.

4. With increasing the number of ARB cycles, the brittle fracture occurred in all the specimens, and dimples were not as deep as in the initial cycle.

References

- [1] Borhani, E., Jafarian, H., Shibata, A., Tsuji, N.: *Mater. Trans.*, *53*, 2012, p. 1863. [doi:10.2320/matertrans.MA201223](https://doi.org/10.2320/matertrans.MA201223)
- [2] Valiev, R. Z., Estrin, Y., Horita, Z., Langdon, T. G., Zehetbauer, M. J., Zhu, Y. T.: *JOM*, *58*, 2006, p. 33. [doi:10.1007/s11837-006-0213-7](https://doi.org/10.1007/s11837-006-0213-7)
- [3] Valiev, R. Z., Krasilnikov, N. A., Tsenev, N. K.: *Mater. Sci. Eng. A*, *137*, 1991, p. 35. [doi:10.1016/0921-5093\(91\)90316-F](https://doi.org/10.1016/0921-5093(91)90316-F)
- [4] Saito, Y., Utsunomiya, H., Tsuji, N., Sakai, T.: *Acta Mater.*, *47*, 1999, p. 579. [doi:10.1016/S1359-6454\(98\)00365-6](https://doi.org/10.1016/S1359-6454(98)00365-6)
- [5] Horita, Z., Smith, D. J., Furukawa, M., Nemoto, M., Valiev, R. Z., Langdon, T. G.: *Journal Mater. Res.*, *11*, 1996, p. 1880. [doi:10.1557/JMR.1996.0239](https://doi.org/10.1557/JMR.1996.0239)
- [6] Richert, J., Richert, M.: *Aluminum*, *62*, 1986, p. 604.
- [7] Schafler, E., Kerber, M. B.: *Mater. Sci. Eng. A*, *462*, 2007, p. 139. [doi:10.1016/j.msea.2005.11.085](https://doi.org/10.1016/j.msea.2005.11.085)
- [8] Saito, Y., Tsuji, N., Utsunomiya, H., Sakai, T., Hong, R. G.: *Script. Mater.*, *39*, 1998, p. 1221. [doi:10.1016/S1359-6462\(98\)00302-9](https://doi.org/10.1016/S1359-6462(98)00302-9)
- [9] Borhani, E., Jafarian, H., Terada, D., Adachi, H., Tsuji, N.: *Mater. Trans.*, *53*, 2012, p. 72. [doi:10.2320/matertrans.MD201125](https://doi.org/10.2320/matertrans.MD201125)
- [10] Borhani, E., Jafarian, H., Sato, T., Terada, D., Miyajima, Y., Tsuji, N.: In: *Proceedings of 12th Conf. Al Alloys*. Eds.: Kumai, S., Umezawa, O., Takayama, Y., Tsuchida, T., Sato, T. Tokyo, The Japan Institute of Light Metals 2010, p. 2168.
- [11] Borhani, E., Jafarian, H., Adachi, H., Terada, D., Tsuji, N.: *Mater. Sci. Forum*, *667–669*, 2011, p. 211. [doi:10.4028/www.scientific.net/MSF.667-669.211](https://doi.org/10.4028/www.scientific.net/MSF.667-669.211)
- [12] Takata, N., Yamada, K., Ikeda, K., Yoshida, F., Nakashima, H., Tsuji, N.: *Mater. Trans.*, *48*, 2007, p. 2043. [doi:10.2320/matertrans.MA200701](https://doi.org/10.2320/matertrans.MA200701)
- [13] Huang, X., Tsuji, N., Hansen, N., Minamino, Y.: *Mater. Sci. Eng. A*, *340*, 2003, p. 265. [doi:10.1016/S0921-5093\(02\)00182-X](https://doi.org/10.1016/S0921-5093(02)00182-X)
- [14] Pirgazi, H., Akbarzadeh, A., Petrov, R., Kestens, L.: *Mater. Sci. Eng. A*, *497*, 2008, p. 132. [doi:10.1016/j.msea.2008.06.025](https://doi.org/10.1016/j.msea.2008.06.025)
- [15] Costa, A. L. M., Reis, A. C. C., Kestens, L., Andrade, M. S.: *Mater. Sci. Eng. A*, *406*, 2005, p. 279. [doi:10.1016/j.msea.2005.06.058](https://doi.org/10.1016/j.msea.2005.06.058)
- [16] Knipling, K. E., Dunand, D. C., Seidman, D. N.: *Acta Mater.*, *56*, 2008, p. 1182. [doi:10.1016/j.actamat.2007.11.011](https://doi.org/10.1016/j.actamat.2007.11.011)
- [17] Humphreys, F. J., Hatherly, M.: *Recrystallization and Related Annealing Phenomena*. New York, Pergamon 2004.
- [18] Knipling, K. E., Dunand, D. C., Seidman, D. N.: *Acta Mater.*, *56*, 2008, p. 114. [doi:10.1016/j.actamat.2007.09.004](https://doi.org/10.1016/j.actamat.2007.09.004)
- [19] Sato, T., Terada, D., Tsuji, N.: *Mater. Sci. Forum*, *584–586*, 2008, p. 728. [doi:10.4028/www.scientific.net/MSF.584-586.728](https://doi.org/10.4028/www.scientific.net/MSF.584-586.728)
- [20] *ASM Metals Handbook: Fractography*. Volume 12. Materials Park, ASM International 1987.
- [21] Tamimi, S., Ketabchi, M., Parvin, N.: *Mater. Design*, *30*, 2009, p. 2556. [doi:10.1016/j.matdes.2008.09.039](https://doi.org/10.1016/j.matdes.2008.09.039)
- [22] Rezaei, M. R., Toroghinejad, M. R., Ashrafizadeh, F.: *Mater. Process. Tech.*, *211*, 2001, p. 1184. [doi:10.1016/j.jimatprotec.2011.01.023](https://doi.org/10.1016/j.jimatprotec.2011.01.023)
- [23] Hertzberg, R. W.: *Deformation and Fracture Mechanics of Engineering Materials*. 3rd Edition. Singapore, John Wiley & Sons Inc. 1989.